T. Luo, M. Xu, C. Colombo
Dynamics and Control of High Area-To-mass Ratio Spacecraft and Its Application to Geomagnetic Exploration
Acta Astronautica, Vol. 145, 2018, p. 424-437
doi:10.1016/j.actaastro.2018.02.015

Dynamics and Control of High Area-to-mass Ratio Spacecraft and Its Application to Geomagnetic Exploration

Tong Luo [a], Ming Xu [b], Camilla Colombo [c]

[a, b] School of Astronautics, Beihang University, Beijing 100191, China.

[c] Department of Aerospace Science and Technology, Politecnico di Milano, Milano 20156, Italy

[a] luotong@buaa.edu.cn. [b] xuming@buaa.edu.cn (Corresponding author). [c] camilla.colombo@polimi.it.

Abstract

This paper studies the dynamics and control of a spacecraft, whose area-to-mass ratio is increased by deploying a reflective orientable surface such as a solar sail or a solar panel. The dynamical system describing the motion of a non-zero attitude angle high area-to-mass ratio spacecraft under the effects of the Earth's oblateness and solar radiation pressure admits the existence of equilibrium points, whose number and the eccentricity values depend on the semi-major axis, the area-to-mass ratio and the attitude angle of the spacecraft together. When two out of three parameters are fixed, five different dynamical topologies successively occur through varying the third parameter. Two of these five topologies are critical cases characterized by the appearance of the bifurcation phenomena. A conventional Hamiltonian structure-preserving (HSP) controller and an improved HSP controller are both constructed to stabilize the hyperbolic equilibrium point. Through the use of a conventional HSP controller, a bounded trajectory around the hyperbolic equilibrium point is obtained, while an improved HSP controller allows the spacecraft to easily transfer to the hyperbolic equilibrium point and to follow varying equilibrium points. A bifurcation control using topologies and changes of behavior areas can also stabilize a spacecraft near a hyperbolic equilibrium point. Natural trajectories around stable equilibrium point and these stabilized trajectories around hyperbolic equilibrium point can all be applied to geomagnetic exploration.

Key Words: High area-to-mass ratio spacecraft, Hyperbolic equilibrium point, Hamiltonian structure-preserving control, Bifurcation control, Geomagnetic exploration

1. Introduction

Orbital eccentricity long-term oscillations have been observed in gentle inclined orbit behaviour of satellites such as the ECHO balloon [1] and Vanguard [2]. This orbital dynamic system can be described by a Hamiltonian function written in two variables, the osculating orbit eccentricity e and the solar angle Φ between the direction of

the orbit pericentre and the direction of Earth-Sun line [3] [4]. At some specific values of the system total energy, there exist three equilibrium points, including one unstable point at $\Phi=\pi$ and two stable points at $\Phi=0$ and $\Phi=\pi$. The equilibrium points at $\Phi=0$ and $\Phi=\pi$ respectively correspond to heliotropic and anti-heliotropic orbits [5][6], which are distinguished by their frozen apse line with respect to the Sun. More specifically, heliotropic orbits maintain their apogee in the direction of the Sun, while anti-heliotropic orbits have their apogee in the direction away from the Sun.

The unstable equilibrium point has two-dimension stable and unstable manifolds of saddle topological type. Therefore, the eccentricity cannot be maintained near this equilibrium point without any control [6]. Scheeres et al. constructed a Hamiltonian structure-preserving (HSP) controller, which can stabilize a system with the feedback of stable and unstable manifolds and was applied to formation flight with low-thrust propulsion [7]. To extend the work of Scheeres et al., HSP controller was improved by adding the feedback of center manifold and releasing the constraints on gains [8]. The modified HSP controller was successfully used in solar sail's circular restricted three body problem [8] and quasi-periodic relative trajectories on a J_2-perturbed mean circular orbit [9]. For an equilibrium point of unstable focus topological type, Soldini et al. [10] also constructed a HSP controller to stabilize the unstable equilibrium point.

Applying HSP controller to anti-heliotropic orbits of high area-to-mass ratio spacecraft dynamical system under the effect of Solar Radiation Pressure (SRP) and the perturbation due to the Earth's oblateness (the J_2 effect), Colombo et al. obtained a bounded trajectory around the controlled unstable equilibrium point [5] [6]. The bounded trajectory can be used as a gateway to transfer to low-eccentricity orbits, where librational motion around the stable equilibrium point is possible, or to high-eccentricity orbits, where the spacecraft naturally decays due to atmospheric drag. These two transfer missions are designed for solar sail with different area-to-mass ratios.

Because the attitude angle of the spacecraft in the study of Colombo et al. [5] [6] has a default value as zero, the effect of the attitude angle on the dynamics is ignored and all possible equilibrium points are restricted at $\Phi=0$ and $\Phi=\pi$. In this paper, we propose the exploitation of equilibrium points of non-zero attitude angle high area-to-mass ratio spacecraft. Influenced by the non-zero attitude angle α between the direction of Sun radiation pressure and the normal direction of the spacecraft reflective surface, the positions of dynamical system's possible equilibrium points are changed into $\Phi=\alpha$ and $\Phi=\alpha+\pi$. The existence and the eccentricity values of these equilibrium points depend on the semi-major axis, the area-to-mass ratio and the attitude angle of the spacecraft. The stable equilibrium point at $\Phi=\alpha$ always exists, but the two equilibrium points at $\Phi=\alpha+\pi$ may not exist. When two of these parameters are fixed, five different topologies of e_x-e_y ($e_x=e\cos\Phi$, $e_y=e\sin\Phi$) phase space successively occur through varying the third parameter. Furthermore, two critical cases of topologies are characterized by the appearance of the bifurcation

phenomena.

With the aim of exploring the Earth's magnetosphere, GeoTail was developed by Japan's ISAS in association with the United States' NASA [11]. To achieve consecutive coverage of the geomagnetic tail, MacDonald et al. [12] and McInnes et al. [13] proposed an artificial apse-line precession of an elliptical orbit with major axis oriented in the Sun-Earth line, which can be accomplished by a small solar sail. Later, Mengali et al. [14] developed an optimal steering law to trade off the apse-line precession capability. Based on the mission and system design requirements from ESA's technology reference studies, Lappas et al. [15] proposed an alternate GeoSail design for the Earth's magnetotail study. In addition, anti-heliotropic elliptical orbits were proposed for the GeoTail mission as long residence time is spent in the Earth's geomagnetic tail, hence enabling to obtain the statistical characterization of plasma under a variety of solar wind conditions [16]-[18].

Applying a conventional controller constructed by Xu et al. [8] and Colombo et al. [6] to stabilize the hyperbolic equilibrium point, we obtain a bounded trajectory. Because conventional HSP controller can just guarantee the stability in the sense of Lyapunov rather than asymptotic stability, the controlled spacecraft can only have a bounded trajectory around the hyperbolic equilibrium point rather than transfer to it. Based on the conventional HSP controller, a stronger HSP controller called improved HSP controller is constructed in this paper. The improved HSP controller uses the further feedback of eccentricity error so that the spacecraft can be controlled to transfer to the hyperbolic equilibrium point. Controlled by the improved HSP controller, spacecraft can follow the trajectory with the varying equilibrium points. Another way to stabilize the spacecraft near hyperbolic equilibrium point is via a bifurcation control, which uses topologies and the change of behaviour areas. The distribution of different behaviour areas in e_x-e_y phase space are closely related to attitude angle or area-to-mass ratio independently. Thus, the spacecraft can transfer from the unstable/stable manifolds into the center manifolds by only changing the attitude angle or the area-to-mass ratio. These stabilized trajectories and the natural stable trajectory around stable equilibrium point all possess characteristics of anti-heliotropic elliptical orbits and can be used for geomagnetic exploration. The paper is organized as follows: **Section 2** explains the orbital dynamics of high area-to-mass ratio spacecraft, **Section 3** proposes three stabilization methods around the hyperbolic equilibrium points, while the application to geomagnetic exploration is described in **Section 4**.

2. Orbital dynamics of high area-to-mass ratio spacecraft

2.1 Dynamical model

The two-body dynamics of a high area-to-mass ratio spacecraft orbiting the Earth is strongly perturbed by the effect of solar radiation pressure and the Earth's oblateness J_2. Supposing that the spacecraft orbit has zero inclination, i.e. the equatorial plane is coincident to the ecliptic, and the effect of the eclipses is neglected, Colombo et al. [5] obtained the simplified planar dynamics for zero attitude angle high area-to-mass ratio spacecraft. With the addition of non-zero attitude angle to this model, the secular rate of change of the orbital elements due to SRP and J_2, i.e. the full planar dynamics is derived as

$$\begin{cases} \dfrac{de}{d\lambda_{sun}} = -C(\cos\alpha)^2 \sin(\Phi-\alpha)\sqrt{1-e^2} \\ \dfrac{d\Phi}{d\lambda_{sun}} = -C\left(\cos\alpha\right)^2 \cos(\Phi-\alpha)\dfrac{\sqrt{1-e^2}}{e} + \dfrac{W}{(1-e^2)^2} - 1 \end{cases}, \tag{1}$$

where e is the osculating orbit eccentricity, Φ is the solar angle between the direction of the orbit pericentre and the direction of Earth-Sun line, α is the attitude angle between the direction of Sun radiation pressure and the normal direction of the spacecraft reflective surface, C is the solar radiation pressure parameter, and W is the oblateness parameter. As shown in Fig 1, Φ has a relationship with $\tilde{\omega}$ and λ_{sun}, i.e. $\Phi = \tilde{\omega} - (\lambda_{sun} - \pi)$. $\tilde{\omega}$ is defined as the longitude of the pericentre and λ_{sun} true longitude of the Sun.

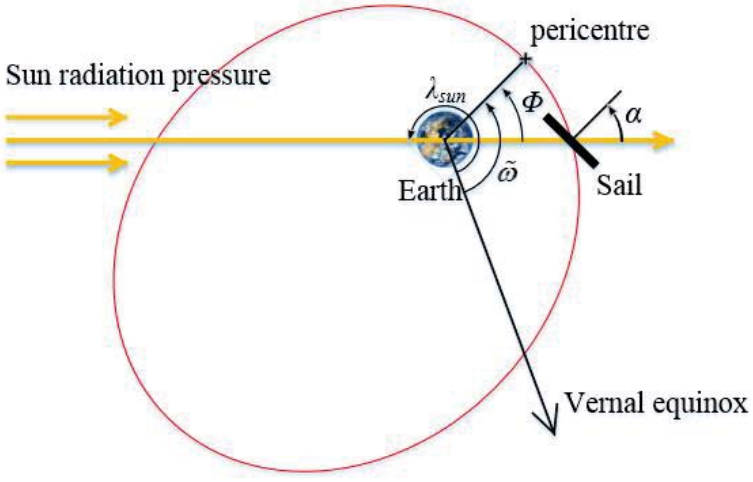

Fig 1. Two-dimensional orbit geometry.

Eq. (1) is governed by parameters C and W, both dependent on the semi-major axis a. The solar radiation pressure parameter is expressed as

$$C = \beta \cdot C^* = \frac{3}{2} p_{\mathrm{SR}} c_R \frac{A_{\mathrm{Sun}}}{m} \frac{a^2}{\mu_{\mathrm{Earth}}} \frac{n}{n_{\mathrm{Sun}}}, \tag{2}$$

where $\beta=A_{Sun}/m$ is defined as the area-to-mass ratio of spacecraft, A_{Sun} is the sail's area exposed to the Sun and m is the mass of the spacecraft; $p_{SR}=4.56\times10^{-6}\mathrm{N/m^2}$ denotes the solar radiation pressure at 1 astronomical unit and c_R is the sail reflectivity coefficient dependent on sail material; a is the semi-major axis, μ_{Earth} is the gravitational constant of the Earth, $n=\sqrt{\mu_{\mathrm{Earth}}/a^3}$ is the spacecraft mean motion, and n_{Sun} is the orbital angular velocity of the Earth around the Sun (circular Earth orbit is adopted).The oblateness parameter W can be expressed as

$$W = \frac{3}{2} J_2 \frac{R_{\mathrm{Earth}}^2}{a^2} \frac{n}{n_{\mathrm{Sun}}}, \tag{3}$$

where $J_2=1.083\times10^{-3}$ is the Earth's second zonal harmonic coefficient, and R_{Earth} is the Earth's mean radius.

The controlled variables in HSP controller are usually of the same physical type. Thus, similarly to Colombo et al. [6], we define the eccentricity vector $\mathbf{e}=[e_x, e_y]^{\mathrm{T}}$, which is given by polar coordinate transformation of e and Φ, i.e. $e_x=e\cos\Phi$, $e_y=e\sin\Phi$. And then Eq. (1) can be equivalently transformed into

$$\begin{cases} \dfrac{de_x}{d\lambda_{sun}} = e_y\left(1-\dfrac{W}{1-e_x^{\,2}-e_y^{\,2}}\right)+\beta\cdot C^*\sqrt{1-e_x^{\,2}-e_y^{\,2}}\left(\cos\alpha\right)^2\sin\alpha \\ \dfrac{de_y}{d\lambda_{sun}} = -e_x\left(1-\dfrac{W}{1-e_x^{\,2}-e_y^{\,2}}\right)-\beta\cdot C^*\sqrt{1-e_x^{\,2}-e_y^{\,2}}\left(\cos\alpha\right)^3 \end{cases}, \tag{4}$$

which will be used to design HSP controller in **Section 3.1**.

2.2 Equilibrium points

Eq. (1) is a typical Hamiltonian system and can be described by following Hamiltonian function

$$H = -\sqrt{1-e^2}+Ce\left(\cos\alpha\right)^2\cos\left(\Phi-\alpha\right)-\frac{W}{3\left(1-e^2\right)^{3/2}}, \tag{5}$$

which allows a maximum of three equilibrium points, i.e. the solutions of following equations

$$\begin{cases} \dfrac{\partial H}{\partial e} = C\left(\cos\alpha\right)^2\cos\left(\Phi-\alpha\right)+\dfrac{e}{\sqrt{1-e^2}}-\dfrac{We}{\left(1-e^2\right)^{5/2}}=0 \\ \dfrac{\partial H}{\partial \Phi} = -C\left(\cos\alpha\right)^2\sin\left(\Phi-\alpha\right)=0 \end{cases}. \tag{6}$$

One stable equilibrium point locates at $\Phi=\alpha$, one stable equilibrium point at $\Phi=\alpha+\pi$ and one hyperbolic equilibrium point at $\Phi=\alpha+\pi$. The existence of these three equilibrium points and their eccentricity values depend on the semi-major axis, the area-to-mass ratio and the attitude angle of the spacecraft.

The geometrical description of phase space is a useful approach to the study of Hamiltonian dynamics [19] [20] .

Here the polar coordinates (e_x, e_y) are chosen to show the trajectory evolution of the spacecraft as Douglas P Hamilton et al. [18] [21] did. Fig 2 shows the trajectory evolution of the spacecraft in e_x-e_y phase space as function of the semi-major axis for given attitude angle and area-to-mass ratio. The equilibrium points always locate on the straight line y=tanα·x in (e_x, e_y) coordinate system. This indicates that the Φ values of equilibrium points are completely determined by spacecraft attitude angle α, i.e. equilibrium points always locate at $\Phi=\alpha$ and $\Phi=\alpha+\pi$. When the spacecraft is placed at low semi-major axis orbit, only one stable equilibrium point at $\Phi=\alpha$ surrounded by center manifolds exist (see the red dots in Fig 2a). Then, the equilibrium points at $\Phi=\alpha+\pi$ appear and separate as the semi-major axis increases (see the red dots in Fig 2b and Fig 2c). Finally, note that not all values of eccentricity are feasible for a given semi-major axis a, since the orbit perigee cannot move below the Earth surface, hence the eccentricity cannot exceed its critical value: $e_{critcal}=1-\frac{R_{earth}}{a}$. The shadow areas in Fig 2 represent the unfeasible trajectory.

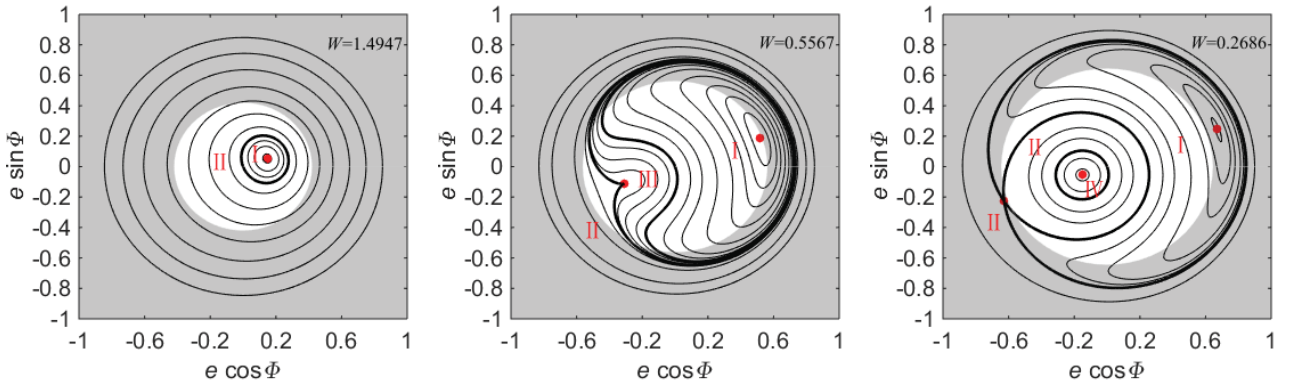

a) a=11000 km, α=20°, β=10 m^2/kg **b)** a=14602 km, α=20°, β=10 m^2/kg **c)** a=18000 km, α=20°, β=10 m^2/kg

Fig 2. e_x-e_y phase space evolution.

Fig 3 summaries all possible eccentricity values of three equilibrium points when area-to-mass ratio is chosen as 10 m^2/kg. Fig 3a shows the eccentricity values of stable equilibrium point at $\Phi=\alpha$, Fig 3b unstable equilibrium point at $\Phi=\alpha+\pi$, and Fig 3c stable equilibrium point at $\Phi=\alpha+\pi$. The separatrices in Fig 3b and Fig 3c represent the critical case (such as Fig 2b) where the stable equilibrium point at $\Phi=\alpha+\pi$ and the unstable equilibrium point at $\Phi=\alpha+\pi$ coincide, and these separatrices divide figures into two parts, i.e. blank area where no equilibrium point exists at $\Phi=\alpha+\pi$ (such as Fig 2a) and colored area where two equilibrium points exist at $\Phi=\alpha+\pi$ (such as Fig 2c). Fig 4 summaries all possible eccentricity values of three equilibrium points when attitude angle is chosen as 20°. Fig 4a shows the eccentricity values of stable equilibrium point at $\Phi=\alpha$, Fig 4b unstable equilibrium point at $\Phi=\alpha+\pi$, and Fig 4c stable equilibrium point at $\Phi=\alpha+\pi$. As in Fig 3, the separatrices in Fig 4b and Fig 4c also represent the critical case and divide the figures into two parts.

As shown in Fig 5, for a given area-to-mass ratio and a given attitude angle, the eccentricity values of stable equilibrium point at $\Phi=\alpha$ and unstable equilibrium point at $\Phi=\alpha+\pi$ increase with the increase of the semi-major axis, while the eccentricity value of stable equilibrium point at $\Phi=\alpha+\pi$ decreases firstly and then increases with the increasing semi-major axis value. As shown in Fig 6, for a given area-to-mass ratio and a given semi-major axis, the eccentricity values of stable equilibrium point at $\Phi=\alpha$ and unstable equilibrium point at $\Phi=\alpha+\pi$ decrease with the increase of attitude angle, while the eccentricity value of the stable equilibrium point at $\Phi=\alpha+\pi$ increases with the increase of attitude angle. As shown in Fig 7, for a given attitude angle and a given semi-major axis, the eccentricity values of stable equilibrium point at $\Phi=\alpha$ and unstable equilibrium point at $\Phi=\alpha+\pi$ increase with the increase of the area-to-mass ratio, while the eccentricity value of the stable equilibrium point at $\Phi=\alpha+\pi$ decreases with the increase of area-to-mass ratio.

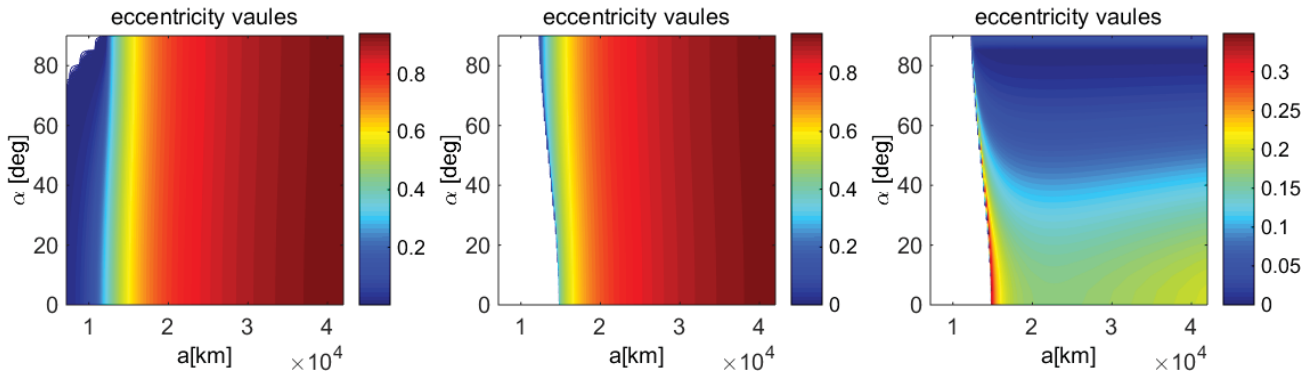

a) β=10 m^2/kg, $\Phi=\alpha$ **b)** β= 10 m^2/kg, $\Phi=\alpha+\pi$, unstable **c)** β=10 m^2/kg, $\Phi=\alpha+\pi$, stable

Fig 3. Eccentricity values of three equilibrium points when area-to-mass ratio is chosen as 10 m^2/kg.

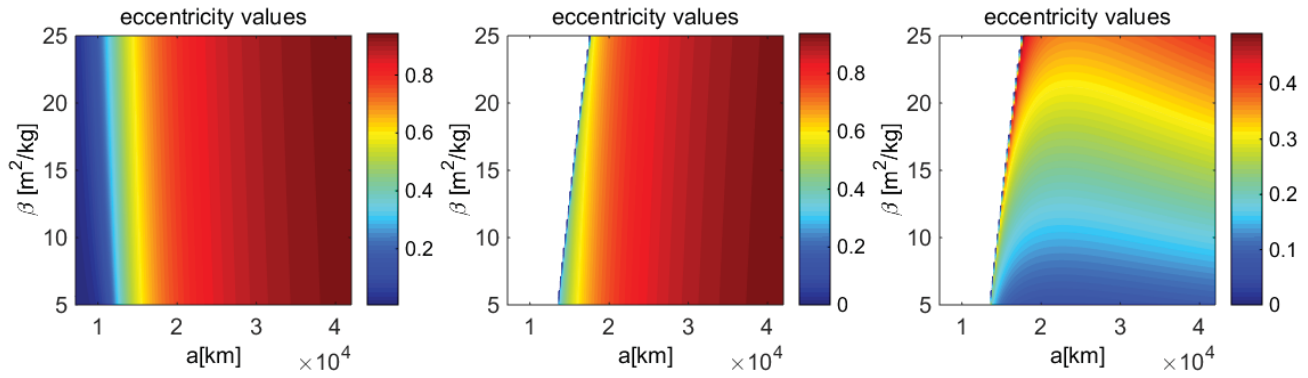

a) α=20˚, $\Phi=\alpha$ **b)** α=20˚, $\Phi=\alpha+\pi$, unstable **c)** α=20˚, $\Phi=\alpha+\pi$, stable

Fig 4. Eccentricity values of three equilibrium points when attitude angle is chosen as 20˚.

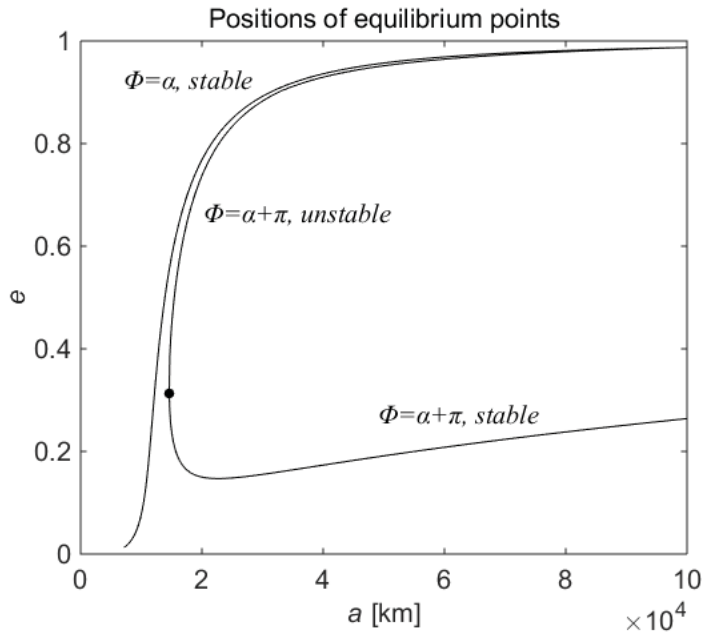

Fig 5. The evolution of the eccentricity values with the semi-major axis, α=20°, β=10 m^2/kg.

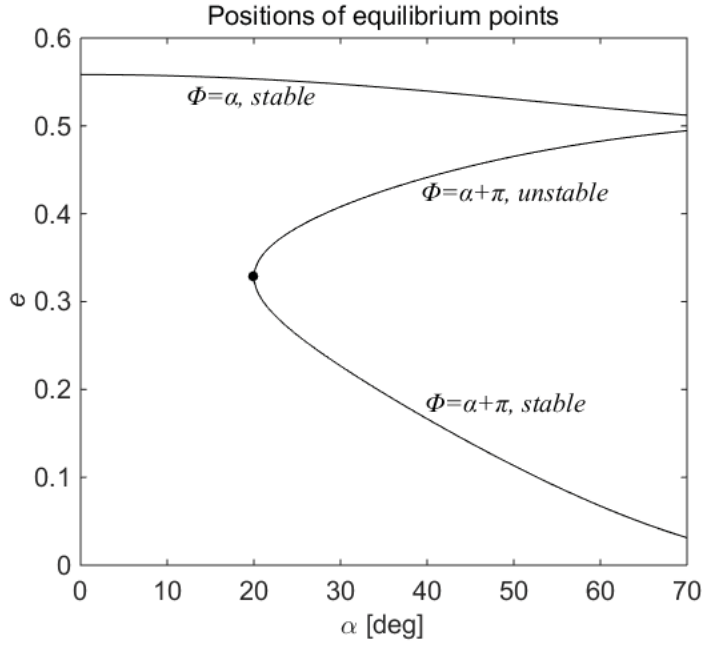

Fig 6. The evolution of the eccentricity values with the attitude angle, a=14602 km, β=10 m^2/kg.

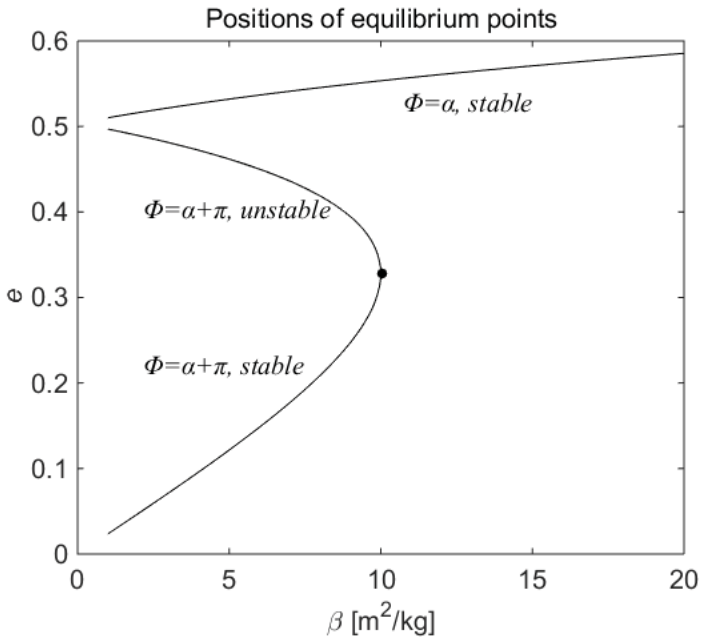

Fig 7. The evolution of the eccentricity values with the area-to-mass ratio, a=14602 *km*, α=20°.

2.3 Topology and bifurcations

As mentioned in **Section 2.2**, the number and topology of equilibrium points in e_x-e_y phase space will change with the semi-major axis, the area-to-mass ratio and the attitude angle of the spacecraft. When two of these parameters are fixed, five different topologies can successively occur through varying the third parameter.

2.3.1Topology changes with semi-major axis

For a given area-to-mass ratio and a given attitude angle, the number of equilibrium points in e_x-e_y phase space increases from one to three with the increasing value of the semi-major axis. The various topologies with different semi-major axes are shown in Fig 8. The topology changes are consistent with the conclusions for the sail with an zero attitude angle by Colombo et al. [6].

The stable equilibrium point is of center type with two-dimension center manifolds, while the unstable equilibrium point is of saddle type with two-dimension stable\unstable manifolds. So there are altogether four different possible behaviors in e_x-e_y phase space: the rotational motion around the stable point at $\Phi=\alpha$ is called behavior I, the extension motion from $\Phi=0$ to $\Phi=2\pi$ is called behavior II, the motion combining the characteristics of behavior I and behavior II around the equilibrium point at $\Phi=\alpha+\pi$ is called behavior III, and the rotational motion around the stable point at $\Phi=\alpha+\pi$ is called behavior IV. The trajectory passing through (0, 0) and the trajectory passing

through the unstable equilibrium point (bold trajectories in Fig 8) are separatrices of these different possible behaviors [17].

In Fig 8a, only one stable equilibrium point at $\Phi=\alpha$ and one separatrix exist, and the separatrix divides the whole e_x-e_y phase space into two areas: behavior I area and behavior II area. In Fig 8b, another equilibrium point at $\Phi=\alpha+\pi$ appears. This equilibrium point possesses characteristics of both stable and unstable equilibrium point, so behavior III appears. And two separatrices divides the whole e_x-e_y phase space into three areas: behavior I area, behavior II area and behavior III area. In Fig 8c, the equilibrium point at $\Phi=\alpha+\pi$ separates into one stable and one unstable equilibrium point, leading to the appearance of behavior IV and homoclinic orbit. Hence, three separatrices divide the whole e_x-e_y phase space into four areas: behavior I area, behavior II area, behavior III area and behavior IV area. In Fig 8d, separatrice passing through (0, 0) and separatrice passing through the unstable equilibrium point overlap, and behavior III area disappears. Therefore, two separatrices divides the whole e_x-e_y phase space into three areas: behavior I area, behavior II area and behavior IV area. In Fig 8e, separatrix passing through (0, 0) and separatrix passing through the unstable equilibrium point separate again, leading to the appearance of another behavior II area. Hence, three separatrices divides the whole e_x-e_y phase space into three areas: behavior I area, behavior II area and behavior IV area.

2.3.2Topology changes with attitude angle

For a given area-to-mass ratio and a given semi-major axis, the number of equilibrium points in e_x-e_y phase space increases from one to three with the increasing value of the attitude angle. There are also altogether four different behaviors which are divided by separatrices in e_x-e_y phase space. The distribution of every behavior area is shown in Fig 9, and the whole process of topology changes is nearly **the** same as that in Fig 8.

2.3.3Topology changes with area-to-mass ratio

For a given semi-major axis and a given attitude angle, the number of equilibrium points in e_x-e_y phase space increases from one to three with the decreasing value of the area-to-mass ratio. There are also altogether four different behaviors which are divided by separatrices in e_x-e_y phase space. The distribution of every behavior area is shown in Fig 10, and the whole process of topology changes is nearly the same as that in Fig 8 and Fig 9.

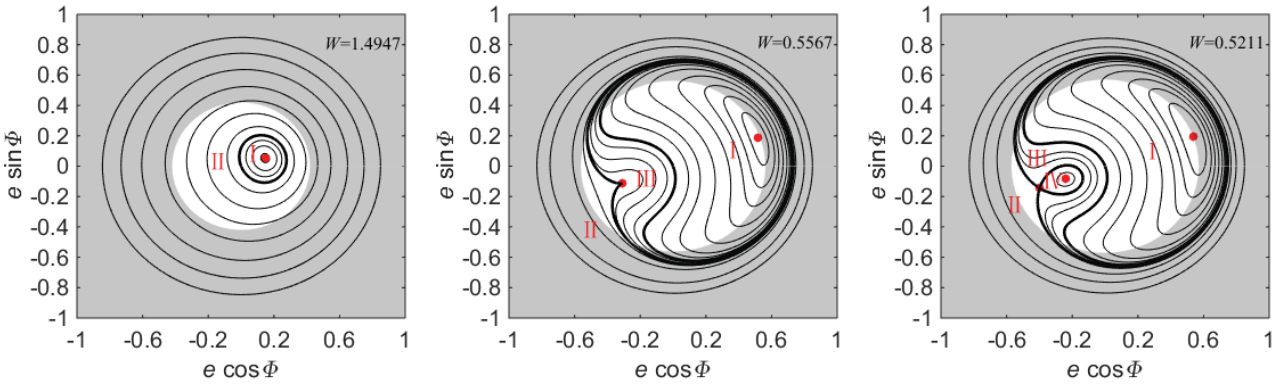

a) a=11000 km, α=20˚, β=10 m^2/kg **b)** a=14602 km, α=20˚, β=10 m^2/kg **c)** a=14881 km, α=20˚, β=10 m^2/kg

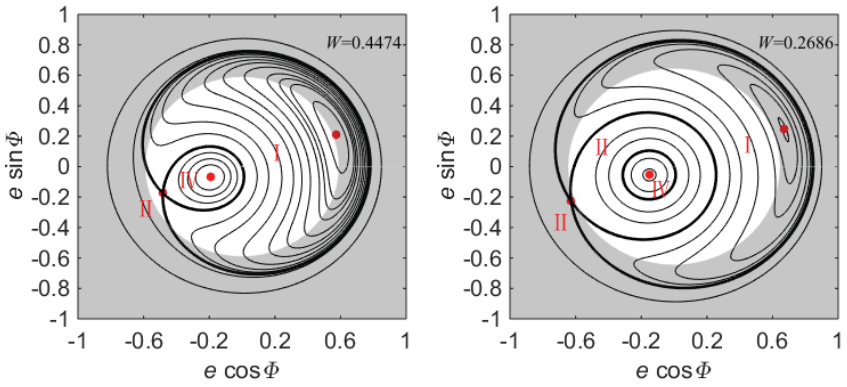

d) a=15563 km, α=20˚, β=10 m^2/kg **e)** a=18000 km, α=20˚, β=10 m^2/kg

Fig 8. Topology changes with semi-major axis for given area-to-mass ratio and attitude angle

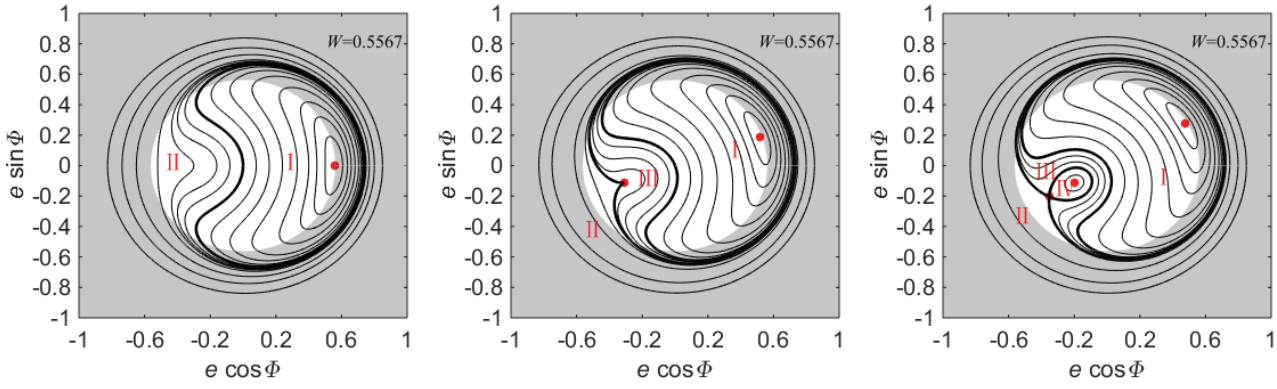

a) a=14602 km, α=0˚, β=10 m^2/kg **b)** a=14602 km, α=20˚, β=10 m^2/kg **c)** a=14602 km, α=30˚, β=10 m^2/kg

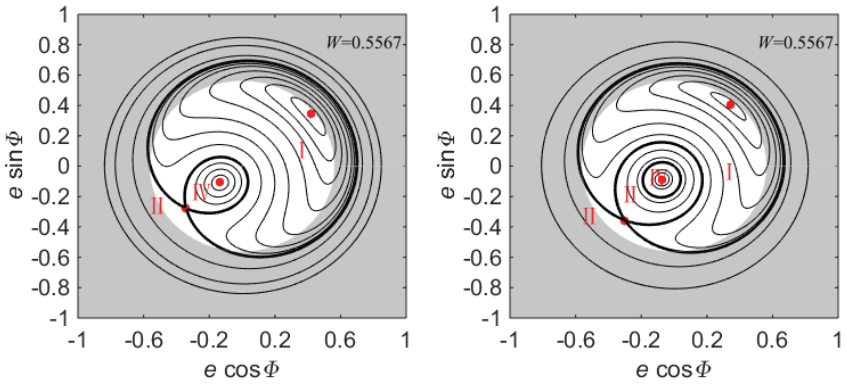

d) a=14602 km, α=39.15°, β=10 m^2/kg **e)** a=14602 km, α=50°, β=10 m^2/kg

Fig 9. Topology changes with attitude angle for given area-to-mass ratio and semi-major axis

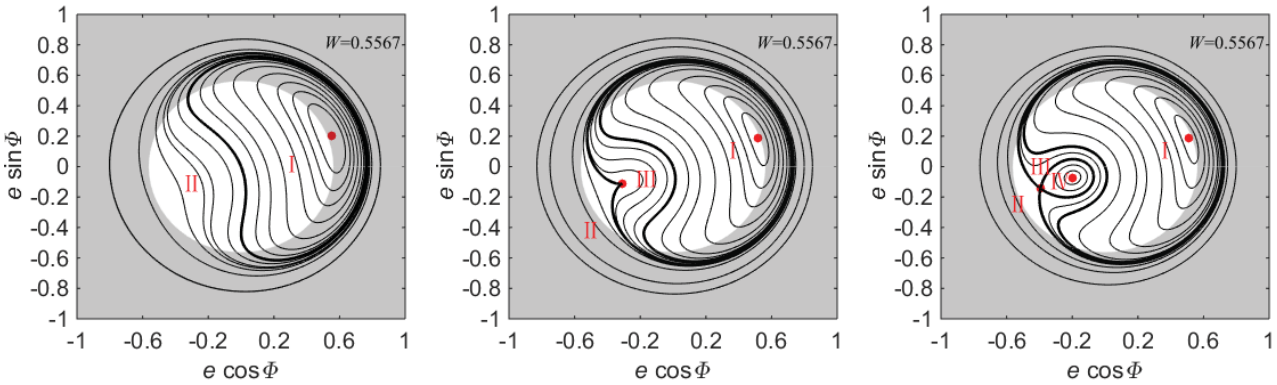

a) a=14602 km, α=20°, β=20 m^2/kg **b)** a=14602 km, α=20°, β=10 m^2/kg **c)** a=14602 km, α=20°, β=8 m^2/kg

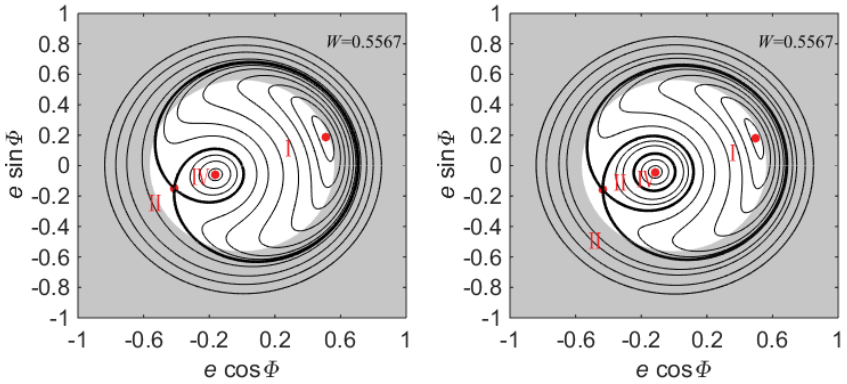

d) a=14602 km, α=20°, β=6.81 m^2/kg **e)** a=14602 km, α=20°, β=5 m^2/kg

Fig 10. Topology changes with area-to-mass ratio for given semi-major axis and attitude angle

2.3.4Conditions for bifurcation phenomena

Among above five different topologies, **b)** and **d)** in Fig 8, Fig 9 or Fig 10 are two critical cases where three parameters must meet a constraint. These critical cases correspond to the appearance of bifurcations.

Bifurcation phenomenon **b)** occurs when the following constraint equations hold

$$\begin{cases} \beta \cdot C^* \cos(\alpha)^2 \dfrac{\sqrt{1-e^2}}{e} + \dfrac{W}{(1-e^2)^2} - 1 = 0 \\ \beta \cdot C^* \cos(\alpha)^2 \dfrac{-1}{e^2\sqrt{1-e^2}} + \dfrac{4e}{(1-e^2)^3} W = 0 \end{cases} . \tag{7}$$

To show the relationship among semi-major axis, area-to-mass ratio and attitude angle, we get a series of numerical solutions from Eq. (7) and obtain the constraint graph of these three parameters. The constraint graph is shown in Fig 11, *x*-axis represents the attitude angle, *y*-axis represents the area-to-mass ratio, and color bar represents the semi-major axis.

Although no constraint equation exists for the bifurcation phenomenon **d)**, the approximate constraint graph of the semi-major axis, the area-to-mass ratio and the attitude angle can be also obtained by traversing all cases. The constraint graph is shown in Fig 12, *x*-axis represents the attitude angle, *y*-axis represents the area-to-mass ratio, and the color bar represents the semi-major axis.

When the area-to-mass ratio, the attitude angle and the semi-major axis are set as the matching values in Fig 11 or Fig 12, bifurcation phenomenon **b)** or **d)** will occur. Two bifurcation phenomena both occur at lower orbit with the increase of attitude angle and the decrease of area-to-mass ratio.

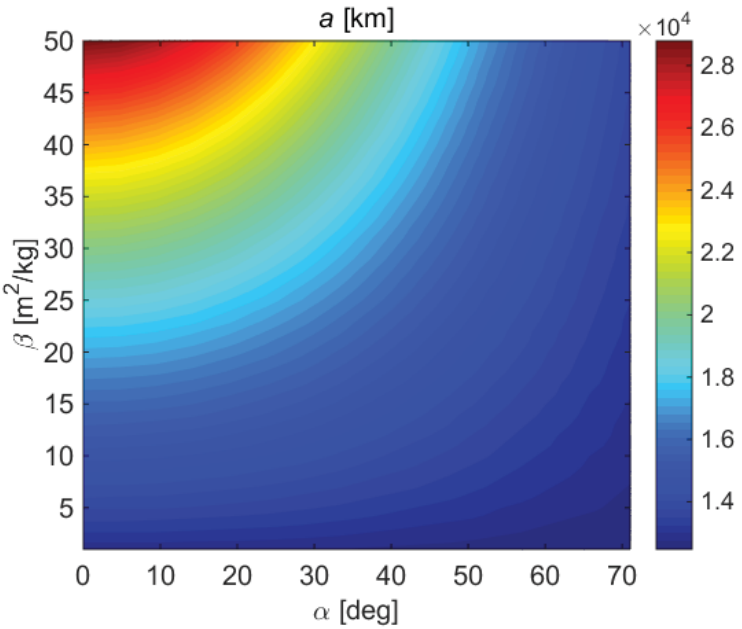

Fig 11. Constraint graph of area-to-mass ratio, attitude angle and semi-major axis for the bifurcation phenomenon b)

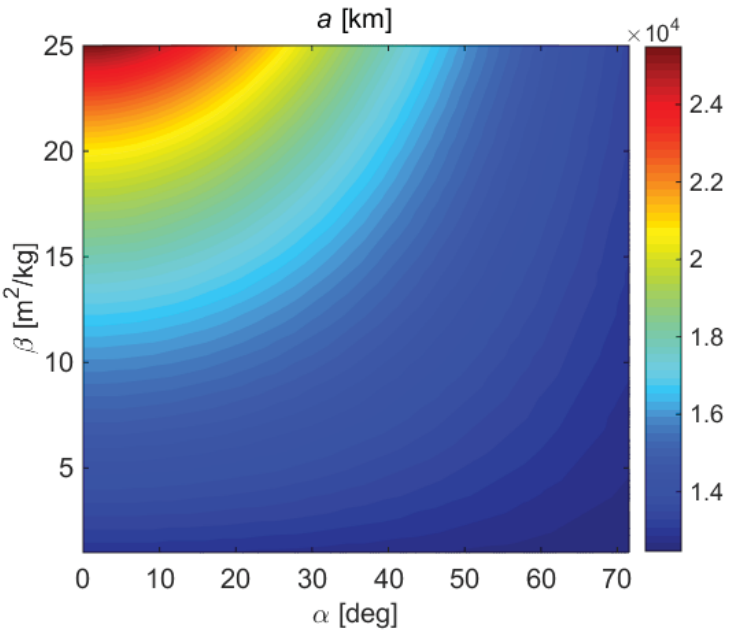

Fig 12. Constraint graph of area-to-mass ratio, attitude angle and semi-major axis for the bifurcation phenomenon d)

3. Stabilization around the hyperbolic equilibrium points

3.1 Conventional Hamiltonian structure-preserving control

The unstable manifold of hyperbolic equilibrium point will bring about spacecraft instability. To stabilize the hyperbolic equilibrium point, a Hamiltonian structure-preserving controller can be constructed as in Xu et al. [8] and Colombo et al. [6], and we call it conventional HSP controller. Bounded trajectory can be generated near the hyperbolic equilibrium point by the conventional HSP controller which feedbacks the difference between the actual eccentricity vector and the eccentricity vector at the hyperbolic equilibrium point. According to the propositions and theorems put forward for the two-dimensional Hamiltonian system [8], the conventional controller can stabilize the system and the poles of the system can be assigned to any different positions on the imaginary axis unless one of the gains G_1 and G_2 is zero, so that the topology type of the hyperbolic equilibrium point is changed from hyperbolic (saddle) to elliptic (center). Furthermore, according to the KAM theory [22] [23], higher-order nonlinear terms will not bring about instability in the controlled Hamiltonian system, so the system with a conventional HSP controller is Lyapunov stable.

The Hamiltonian function satisfies the following constraint condition at hyperbolic equilibrium point [6]

$$H_{e_x e_x} \cdot H_{e_y e_y} - H_{e_x e_y}^2 < 0 . \tag{8}$$

Therefore, the eccentricity vector at hyperbolic equilibrium point $\mathbf{e}_{\text{hyp}} = [e_{x\,\text{hyp}}, e_{y\,\text{hyp}}]^T$ can be solved through Eqs. (6) and (8). As mentioned in **Section 2.1**, the HSP controller is designed based on dynamical system Eq.(4), the linearized form of which near the hyperbolic equilibrium point can be expressed as [6]

$$\frac{d(\mathbf{e}-\mathbf{e}_{\text{hyp}})}{d\lambda_{\text{Sun}}} = \begin{bmatrix} \dfrac{\partial f_{e_x}}{\partial e_x} & \dfrac{\partial f_{e_x}}{\partial e_y} \\ \dfrac{\partial f_{e_y}}{\partial e_x} & \dfrac{\partial f_{e_y}}{\partial e_y} \end{bmatrix} \begin{bmatrix} e_x - e_{x\,\text{hyp}} \\ e_y - e_{y\,\text{hyp}} \end{bmatrix}. \tag{9}$$

To simplify the formulation, the matrix associated to Eq. (9) is denoted as **A**. The hyperbolic eigenvalues of **A** are denoted as $\pm\sigma$, and the stable\unstable manifolds are denoted as $\mathbf{u}_{\pm}$. Then, the conventional controller is constructed as [6]

$$\mathbf{T} = -\sigma^2 \left[G_1 \mathbf{u}_+ \mathbf{u}_+^T + G_2 \mathbf{u}_- \mathbf{u}_-^T \right] \cdot \left(\mathbf{e} - \mathbf{e}_{\text{hyp}} \right), \tag{10}$$

where G_1 and G_2 are the control gains of the unstable and stable manifolds respectively.

The acceleration required by the conventional HSP controller can be obtained by orientating the spacecraft attitude angle α and altering the spacecraft area-to-mass ratio β together [8]. The allocation law of the control is expressed as

$$\partial\mathbf{\Theta} = \left. \frac{\partial \mathbf{f}(\alpha,\beta)}{\partial \mathbf{\Theta}} \right|^{-1}_{(\alpha_0,\beta_0)} \cdot \mathbf{T}, \tag{11}$$

where $\mathbf{\Theta}=[\alpha \quad \beta]^T$ is the control parameter vector, (α_0, β_0) is a pair standard value of spacecraft parameters, $\mathbf{f}(\alpha, \beta)$ is the matrix form of right-hand side of Eq. (4) and the Jacobian is

$$\frac{\partial \mathbf{f}(\alpha,\beta)}{\partial \mathbf{\Theta}} = \left[\frac{\partial \mathbf{f}(\alpha,\beta)}{\partial \alpha} \quad \frac{\partial \mathbf{f}(\alpha,\beta)}{\partial \beta} \right] = C^* \sqrt{1-e_x^{\,2}-e_y^{\,2}} \begin{bmatrix} \beta\cos\alpha\left(1-3(\sin\alpha)^2\right) & (\cos\alpha)^2\sin\alpha \\ -3\beta(\cos\alpha)^2\sin\alpha & -(\cos\alpha)^3 \end{bmatrix}. \tag{12}$$

3.2 Improved Hamiltonian structure-preserving control

Because the conventional HSP controller can just guarantee the stability in the sense of Lyapunov rather than asymptotic stability, the controlled spacecraft can only have a bounded trajectory around the hyperbolic equilibrium point rather than transfer to it. To make it possible for the spacecraft to transfer to the hyperbolic equilibrium point, we constructed a stronger HSP controller and call it improved HSP controller. Based on Eq. (10), the improved controller is constructed as

$$\mathbf{T}^* = \mathbf{T} - k\mathbf{I} \cdot (\mathbf{e} - \mathbf{e}_{\text{hyp}}), \tag{13}$$

where **I** is a two-dimensional identity matrix, and k is a constant coefficient of the controller.

With a controller added to the right-hand side of Eq. (9), the linear dynamical system with the conventional or improved HSP controller can be respectively expressed as

$$\frac{d(\mathbf{e}-\mathbf{e}_{\mathbf{hyp}})}{d\lambda_{\mathrm{Sun}}}=\mathbf{B}\cdot\left(\mathbf{e}-\mathbf{e}_{\mathrm{hyp}}\right), \tag{14}$$

where $\mathbf{B}=\mathbf{A}-\sigma^2\left[G_1\mathbf{u}_+\mathbf{u}_+^T+G_2\mathbf{u}_-\mathbf{u}_-^T\right]$, or

$$\frac{d(\mathbf{e}-\mathbf{e}_{\mathbf{hyp}})}{d\lambda_{\mathrm{Sun}}}=\mathbf{B}^*\cdot\left(\mathbf{e}-\mathbf{e}_{\mathrm{hyp}}\right), \tag{15}$$

where $\mathbf{B}^*=\mathbf{A}-\sigma^2\left[G_1\mathbf{u}_+\mathbf{u}_+^T+G_2\mathbf{u}_-\mathbf{u}_-^T\right]-k\cdot\mathbf{I}$.

According to the mathematic proof for conventional HSP controller [8], **A** has a pair of real eigenvalues and **B** has a pair of imaginary eigenvalues. By noticing that two diagonal elements in **A** and **B** are both opposite numbers, the matrix **B** can be rewritten as

$$\mathbf{B}=\begin{bmatrix}-d & c\\ b & d\end{bmatrix}, \tag{16}$$

and these matrix elements satisfy following constraint condition

$$d^2+bc<0. \tag{17}$$

For improved controller, $\mathbf{B}^*$ can be rewritten as

$$\mathbf{B}^*=\begin{bmatrix}-d-k & c\\ b & d-k\end{bmatrix}, \tag{18}$$

where the two eigenvalues of $\mathbf{B}^*$ are $-k\pm\sqrt{-(d^2+bc)}\cdot i$. When k=0, the improved controller degenerates into the conventional controller in Eq (10); when k<0, two eigenvalues both have positive real part and the topology type of the hyperbolic equilibrium point is changed from saddle to unstable focus. Thus, the improved controller fails to stabilize the original system; when k>0, two eigenvalues both have negative real part and the topology type of the hyperbolic equilibrium point is changed from saddle to stable focus. Thus, the improved controller successes to stabilize the original system. Furthermore, differently from the Lyapunov stability achieved by conventional controller, the change of topology type from saddle to stable focus indicates that the system with an improved controller is asymptotically stable. Hence, the spacecraft can be easily controlled to transfer to the hyperbolic equilibrium point. In addition, the closing speed is determined by the absolute value of k, the greater the absolute

value of k is, the bigger the closing speed is.

The acceleration required by the improved HSP controller can be also obtained by orientating the spacecraft attitude angle α and altering the spacecraft area-to-mass ratio β together. The allocation law of the control has a similar form of Eq. (11), simply replacing **T** with $\mathbf{T}^*$.

3.3 Bifurcation control

The topologies and the distribution of different behavior areas will change with the attitude angle or the area-to-mass ratio. For two different attitude angles or area-to-mass ratios, there may be an overlap area of two different behavior areas. Thus, the spacecraft can transfer from behavior III area (unstable\stable manifolds) into behavior IV area (center manifolds) by only altering the attitude angle or the area-to-mass ratio.

As shown in Fig 13, the distribution of behavior areas in e_x-e_y phase space is different for two different attitude angles, and the overlap part between behavior III area for one attitude angle and behavior IV area for another attitude angle is filled with stars. A similar phenomenon occurs for two different area-to-mass ratios and is shown in Fig 14. When a spacecraft is firstly placed in behavior III area and moves to the overlap area, it can immediately transfer to behavior IV area by a sudden change of the attitude angle or the area-to-mass ratio. Then the spacecraft will have a stable trajectory around the new stable equilibrium point.

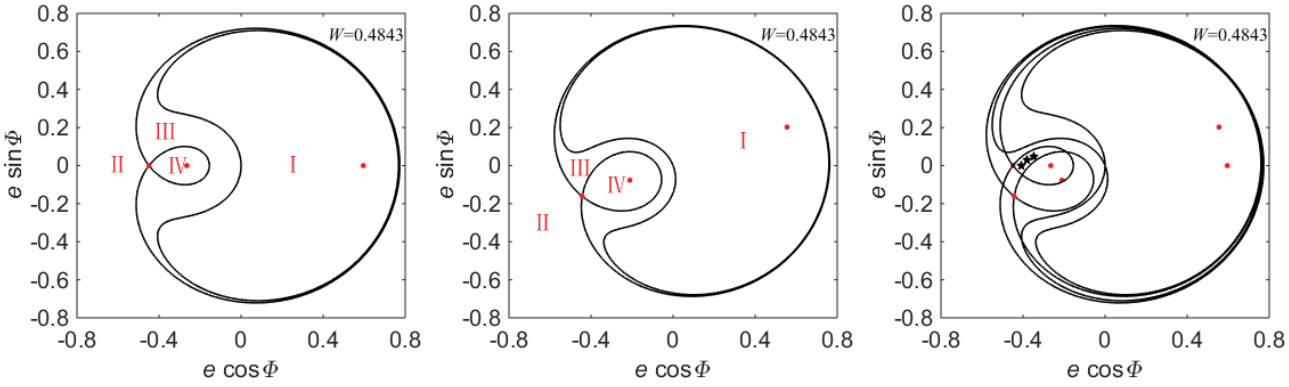

a=15200 km, α=0°, β=10 m^2/kg a=15200 km, α=20°, β=10 m^2/kg Overlap part with stars

Fig 13. Overlap part between behavior III area and behavior IV area for two different attitude angles.

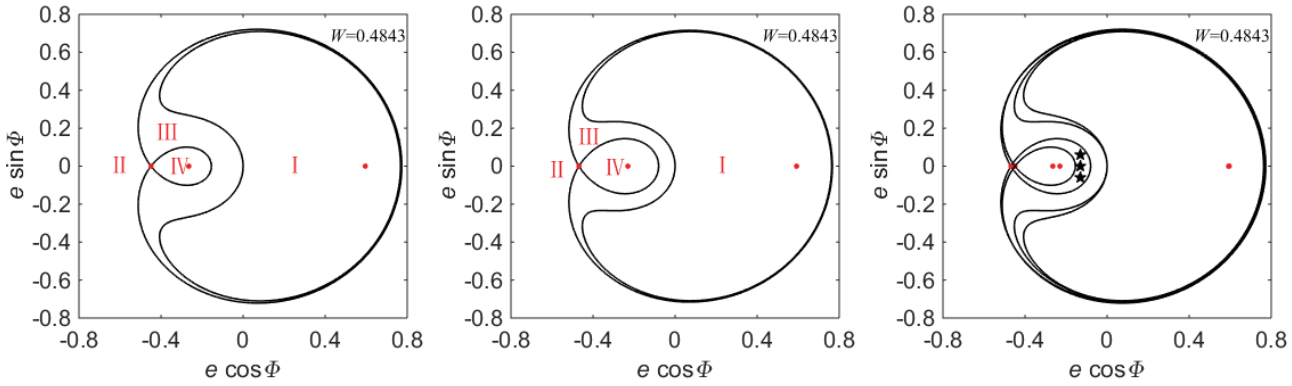

a=15200 km, α=0°, β=10 m^2/kg a=15200 km, α=0°, β=9 m^2/kg Overlap part with stars

Fig 14. Overlap part between behavior III area and behavior IV area for two different area-to-mass ratios

A bifurcation control achieved by changing attitude angle is designed as follows:

$$\alpha = \begin{cases} \alpha_o & t < T \\ \alpha_T & t > T \end{cases}, \tag{19}$$

where T is the time when the maneuver is performed, α_0 is the initial attitude angle and α_T is the final attitude angle.

A bifurcation control achieved by changing area-to-mass ratio is designed as follows:

$$\beta = \begin{cases} \beta_o & t < T \\ \beta_T & t > T \end{cases}, \tag{20}$$

where T is the time when the maneuver is performed, β_0 is the initial area-to-mass ratio and β_T is the final area-to-mass ratio.

Compared to the HSP control, the bifurcation control cannot change an unstable equilibrium point into a stable one. However, a spacecraft with a bifurcation control can also be stabilized by transferring to the center manifolds of new stable equilibrium point. In addition, only one control parameter is involved in bifurcation control and controller form is very simple. The HSP control is a continuous control, while the bifurcation control is a transient control. Therefore, several bifurcation controls may be required at different moments to complete a practical mission.

4. Application to geomagnetic exploration

A spacecraft can stay in geomagnetic area for a long time when moving on an anti-heliotropic elliptical orbit. As shown in Fig 15, the whole geomagnetic area can be covered by high area-to-mass ratio spacecraft through setting different attitude angles and semi-major axes. According to the properties of dynamics, an unstable equilibrium point at $\Phi=\alpha+\pi$ always has a larger eccentricity value than stable equilibrium point at $\Phi=\alpha+\pi$. Thus the controlled orbits

around an unstable equilibrium point are preferred for geomagnetic exploration. However, when the semi-major axis is too large, the unstable equilibrium point is in a shadow area where the spacecraft will collide with Earth. Thus, bounded trajectories around an unstable equilibrium point can be simply used to explore magnetic field near Earth, but cannot be used to explore magnetotail. Noticing that the eccentricity of stable equilibrium point will decrease firstly and then increase with the increase of semi-major axis, we can directly use bounded trajectories around a stable equilibrium point to explore the magnetotail when the area-to-mass ratio and the semi-major axis are set large enough.

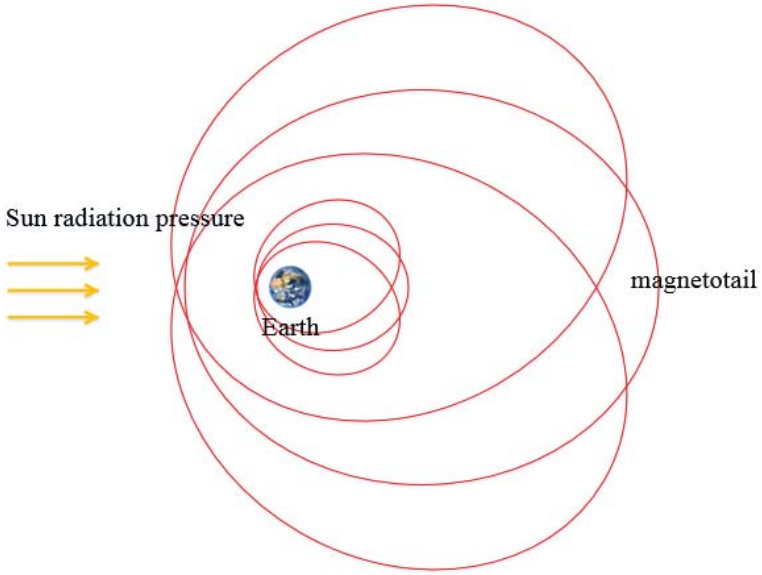

Fig 15. Anti-heliotropic elliptical orbits for geomagnetic exploration

4.1 Natural orbit for exploring magnetotail

Suppose that a spacecraft with 30 m^2/kg area-to-mass ratio and zero attitude angle is initially placed into an elliptical orbit with a semi-major axis of 120000 km, an eccentricity of 0.9, and a solar angle of 165°. Then the spacecraft will motion around the stable equilibrium point and cover a selected region of the magnetotail. The trajectories in the e_x-e_y phase space is shown in Fig 16. Because the values of e and Φ of the spacecraft orbits have a periodic change, the intersection points of the spacecraft orbits and the Sun-Earth line also have a periodic change. Some spacecraft orbits are shown in Fig 17, and the variation of the distance from the Earth to the intersection points is shown in Fig 18.

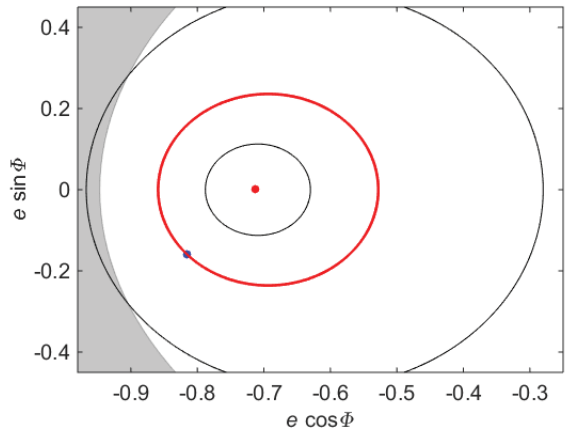

Fig 16. Exploration mission of magnetotail by natural orbits.

Spacecraft initial parameters: a=120000 km, e=0.9, Φ=165°, β=30 m^2/kg, α=0°.

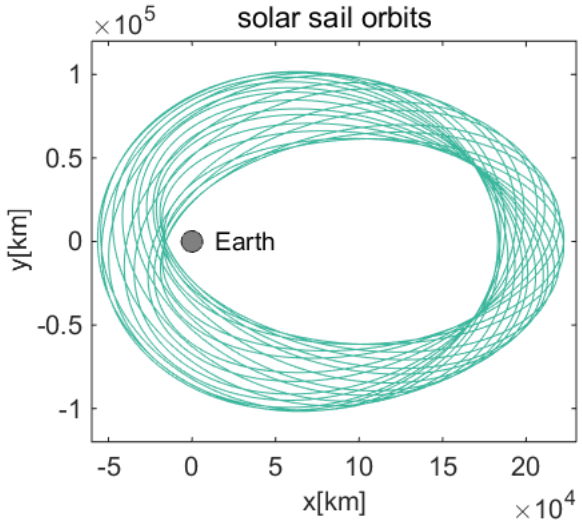

Fig 17. Spacecraft orbits around the Earth.

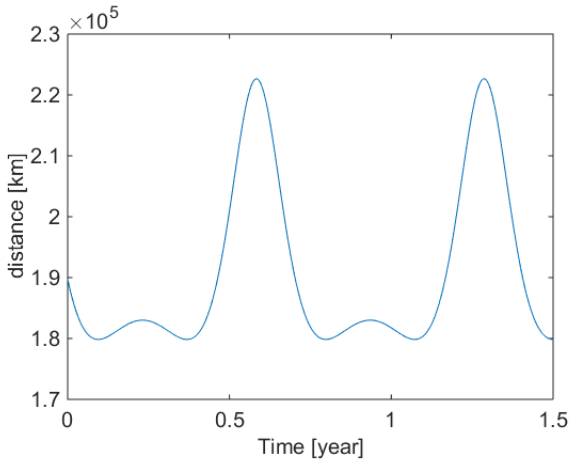

Fig 18. Distance from the Earth to the intersection points.

4.2 Controlled orbits for exploring the magnetic field near the Earth

According to **Section 3**, a spacecraft can be controlled around the unstable equilibrium point by three different methods. In following sections, controlled orbits by these methods are all used to explore the magnetic field near the Earth.

4.2.1. Orbit controlled by conventional HSP controller

Suppose that a spacecraft with 10 m^2/kg area-to-mass ratio and zero attitude angle is initially placed into an elliptical orbit with a semi-major axis of 16206 km, an eccentricity of 0.6, and a solar angle of 165°. After this spacecraft moves naturally for 0.5 years, a conventional HSP controller with control gains set to G_1=2 and G_2=-2 is applied to this spacecraft so that a bounded trajectory is obtained to cover a selected region of magnetic field near Earth.

The exploration composed by three sections is designed as the phase trajectory in Fig 19: (1) the blue line represents the natural motion before control is applied; (2) the red line represents the bounded trajectory around the unstable equilibrium point under the effect of control; (3) the green line represents the natural motion reentering to the Earth's atmosphere without control. Because the values of e and Φ of the spacecraft orbits during control have a periodic change, the intersection points of the spacecraft orbits and the Sun-Earth line also have a periodic change. Some spacecraft orbits are shown in Fig 20 and the whole variation of the distance from the Earth to the intersection points during control is shown in Fig 21.

The conventional HSP control changes the topology type of the equilibrium point from saddle to center. Thus, the controlled spacecraft can have a bounded trajectory (namely the red line in Fig 19) around the hyperbolic equilibrium point. However, the specific position of the bounded trajectory in the phase space is uncontrolled. It is almost impossible to obtain a bounded trajectory which can be completely consistent with the required trajectory. In addition, the acceleration required by this controller should be obtained by orientating the attitude angle and altering the area-to-mass ratio together. Continuously varying attitude angle and area-to-mass ratio are necessary to complete this control mission.

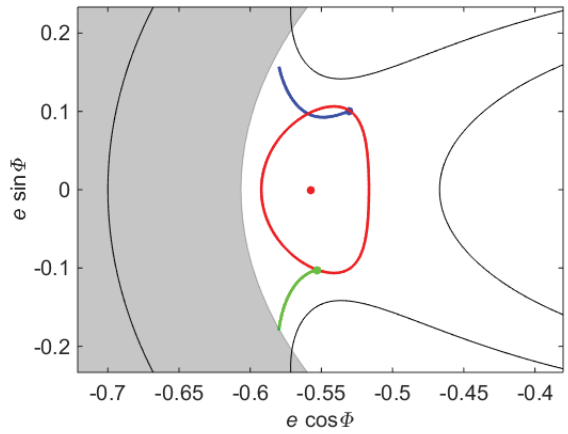

Fig 19. Exploration mission of the magnetic field near the Earth by using conventional HSP controller. Control gains: G_1=2, G_2=-2. Spacecraft initial parameters: a=16206 km, e=0.6, Φ=165°, β=10 m^2/kg, α=0°.

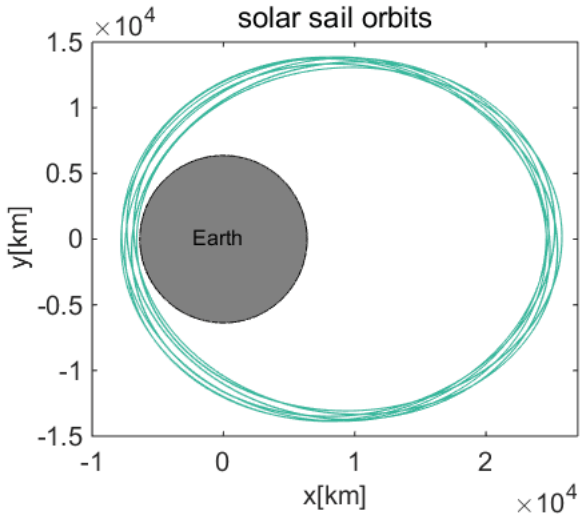

Fig 20. Spacecraft orbits around the Earth during control.

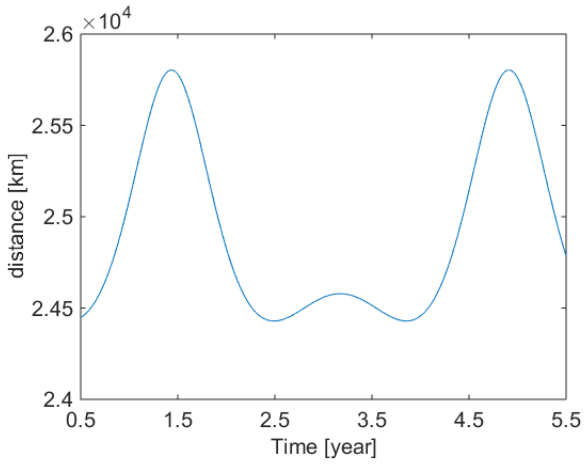

Fig 21. Distance from the Earth to the intersection points during control.

4.2.2. Orbit controlled by the improved HSP controller

A series of unstable equilibrium points can be obtained by varying the attitude angle of the spacecraft The change range of the attitude angle can be designed to cover an intended region of the magnetic field near the Earth. In addition, the spacecraft can easily transfer to an unstable equilibrium point by improved HSP controller, and when the position of unstable equilibrium point is changed, spacecraft will transfer to the new point quickly. So, a spacecraft with improved HSP control can track these changing equilibrium points and complete the geomagnetic exploration.

Supposing that a spacecraft with 10 m^2/kg area-to-mass ratio and -20° attitude angle is initially placed into an elliptical orbit with a semi-major axis of 15834 km, an eccentricity of 0.55, and a solar angle of 145°. An improved HSP controller with control gains set to G_1=2, G_2=-2 and k=10 is applied to this spacecraft. A change rule of attitude angle is designed as follows

$$\alpha = \begin{cases} \alpha_0 & t < T_1 & G_1 = 0, G_2 = 0, k = 0 \\ \alpha_0 & T_1 \le t \le T_2 & G_1 = 2, G_2 = -2, k = 10 \\ \alpha_0 \cos(t - T_2) & T_2 \le t \le T_3 & G_1 = 2, G_2 = -2, k = 10 \\ \alpha_0 & t > T_3 & G_1 = 0, G_2 = 0, k = 0 \end{cases}, \tag{21}$$

where α_0=-20° is the initial and final attitude angle, T_1=π TU (i.e. 0.5 years) is the time spent before controller is applied, T_2=3π TU (i.e. 1.5 years) is the time spent before attitude angle changes, T_3=6π TU (i.e. 3 years) is the moment when the controller is turned off.

The exploration composed by four sections is designed as the phase trajectory in Fig 22: (1) the blue line represents the natural motion before control is applied; (2) the yellow line represents the transfer trajectory to the initial unstable equilibrium point under the effect of control; (3) the red line represents the tracking trajectory with varying attitude angle; (4) the green line represents the natural motion falling to the Earth without control. Because the values of e and Φ of the spacecraft orbits during control have a periodic change, the intersection points of the spacecraft orbits and the Sun-Earth line also have a periodic change. Some spacecraft orbits are shown in Fig 23 and the whole variation of the distance from the Earth to the intersection points during control is shown in Fig 24.

The improved HSP control changes the topology type of the equilibrium point from saddle to stable focus. The controlled spacecraft can transfer to the hyperbolic equilibrium point (namely the yellow line in Fig 22) and follow the changing hyperbolic equilibrium points (namely the red line Fig 22). Therefore, the specific trend of tracking trajectory (namely the red line Fig 22) can be controlled. When the changing trajectory of hyperbolic equilibrium points is designed the same as the required trajectory, the controlled spacecraft will follow the required trajectory. Because the improved HSP control needs further feedback of eccentricity vector error, in general, lager varying values

of attitude angle and area-to-mass ratio are needed compared to the conventional HSP control.

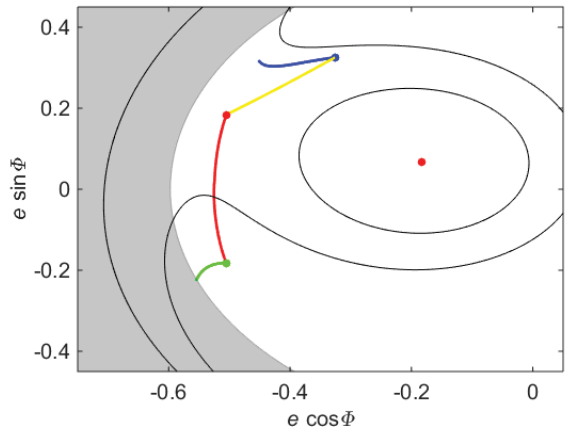

Fig 22. Exploration mission of the magnetic field near the Earth by using improved HSP controller. Control gains: G_1=2, G_2=-2, k=10. Spacecraft initial parameters: a=15834 km, e=0.55, Φ=145°, β=10 m^2/kg, α=-20°.

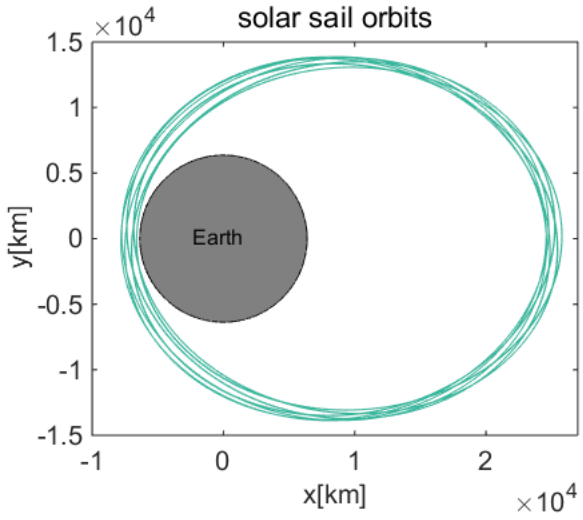

Fig 23. Spacecraft orbits around the Earth during control.

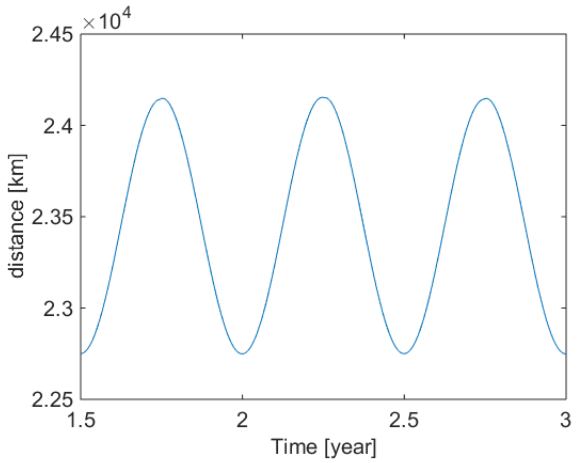

Fig 24. Distance from the Earth to the intersection points during control.

4.2.3. Orbit controlled by attitude angle

When a spacecraft is initially placed in behavior III area, it can transfer into behavior IV area by changing its attitude angle, and then the spacecraft will have bounded trajectory in the e_x-e_y phase space. Like bounded trajectory obtained by conventional HSP control, this natural bounded trajectory can also complete exploration of the magnetic field near the Earth.

Suppose that a spacecraft with 10 m^2/kg area-to-mass ratio and 20° attitude angle is initially placed into an elliptical orbit with a semi-major axis of 15160 km, an eccentricity of 0.55, and a solar angle of 175°. A bifurcation control completed by changing the attitude angle is applied to spacecraft to transfer into the center manifolds, and another similar controller is applied to spacecraft to transfer into a high-eccentricity orbit. The whole control process is expressed as

$$\alpha = \begin{cases} \alpha_o & t < T_1 \\ \alpha_1 & T_1 < t < T_2 \\ \alpha_2 & t > T_2 \end{cases}, \tag{22}$$

where α_0=20° is the initial attitude angle, α_2=-20° is the final attitude angle, α_1=0° is the attitude angle when spacecraft in the center manifolds, T_1=2π TU (i.e. 1 year) and T_2=14π TU (i.e. 7 years) are two maneuver moments.

The exploration composed by three sections is designed as the phase trajectory in Fig 25: (1) the blue line represents the natural motion before the attitude angle changed; (2) the red line represents the bounded trajectory around new stable equilibrium point after the first change of attitude angle; (3) the green line represents the natural motion falling to the Earth after the second change of the attitude angle. Because the values of e and Φ of the spacecraft orbits between the two maneuvers have a periodic change, the intersection points of the spacecraft orbits

and the Sun-Earth line also have a periodic change. Some spacecraft orbits are shown in Fig 26 and the variation of the distance from the Earth to the intersection points between the two maneuvers is shown in Fig 27.

Compared to the HSP control, the bifurcation control cannot change an unstable equilibrium point into a stable one. However, a spacecraft with a bifurcation control can also be stabilized by transferring to the center manifolds of new stable equilibrium point. In addition, only one control parameter is involved in bifurcation control and controller form is very simple. The HSP control is a continuous control, while the bifurcation control is a transient control. Therefore, several bifurcation controls may be needed at different moments to complete a practical mission.

The bifurcation control completed by changing the attitude angle cannot change the topology type of the equilibrium point. The controlled spacecraft is stabilized by transferring to the center manifolds of a new stable equilibrium point. This control is achieved by only varying the attitude angel and the control strategy is very simple. However, this control is instantaneously completed, which requires good respond speed of actuators.

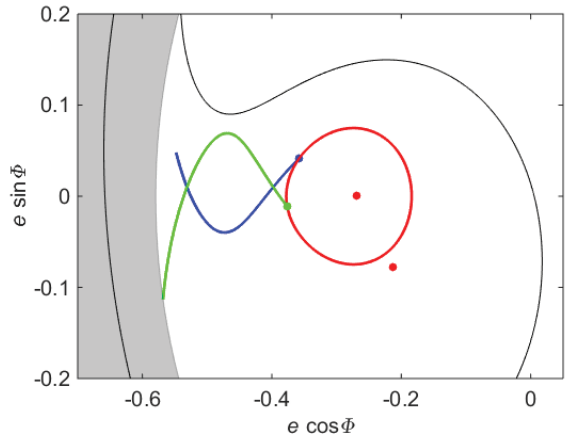

Fig 25. Exploration mission of the magnetic field near the Earth by bifurcation control completed by changing the attitude angle. Spacecraft initial parameters: a=15160 km, e=0.55, Φ=175°, β=10 m^2/kg, α=20°.

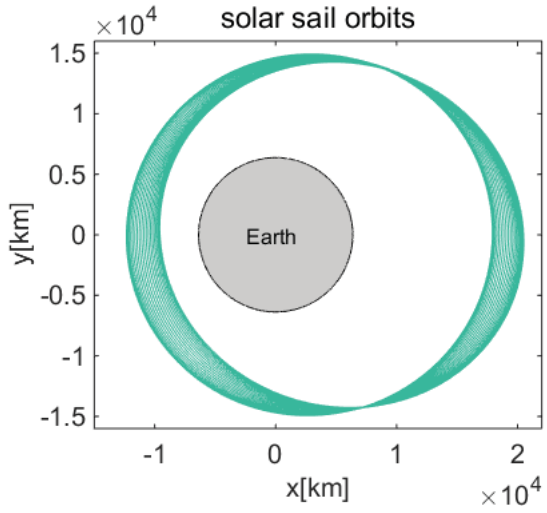

Fig 26. Spacecraft orbits around the Earth between the two maneuvers.

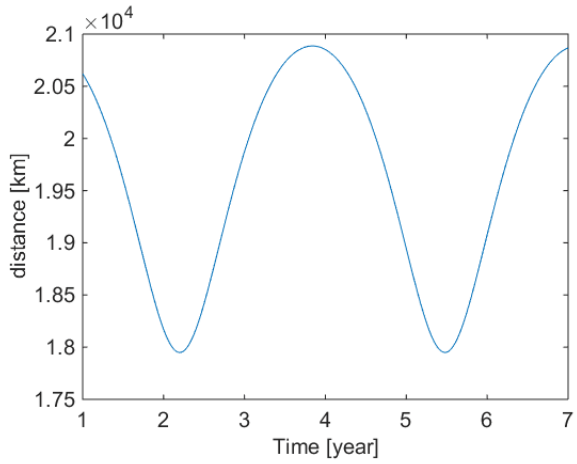

Fig 27. Distance from the Earth to the intersection points between the two maneuvers.

4.2.4. Orbit controlled by area-to-mass ratio

When a spacecraft is initial placed in behavior III area, it can also transfer into behavior IV area by changing its area-to-mass ratio, and then the spacecraft will have a bounded trajectory in e_x-e_y phase space, which can also complete exploration mission of magnetic field near Earth.

Suppose that a spacecraft with 10 m^2/kg area-to-mass ratio and zero attitude angle is initially placed into an elliptical orbit with a semi-major axis of 14881 km, an eccentricity of 0.55, and a solar angle of 145°. A bifurcation control completed by changing the area-to-mass ratio is applied to spacecraft to transfer into the center manifolds, and another similar controller is applied to the spacecraft to transfer into a high-eccentricity orbit. The whole control process is expressed as

$$\beta = \begin{cases} \beta_o & t < T_1 \\ \beta_1 & T_1 < t < T_2 \\ \beta_0 & t > T_2 \end{cases}, \tag{23}$$

where β_0=10 m^2/kg is the initial and final area-to-mass ratio, β_1=8 m^2/kg is the area-to-mass ratio when the spacecraft in the center manifolds, T_1=3π TU (i.e. 1.5 years) and T_2=10π TU (i.e. 5 year) are two maneuver moments. Such a control can be achieved by changing the area of the sail as proposed in Soldini et al. [10] or by changing the reflectivity coefficient of the sail via electrochromic coating, as proposed in Lücking et al. [17].

The exploration composed by three sections is designed as the phase trajectory in Fig 28: (1) the blue line represents the natural motion before area-to-mass ratio changed; (2) the red line represents the bounded trajectory around new stable equilibrium point after the first change of area-to-mass ratio; (3) the green line represents the natural motion reentering to the Earth after the second change of area-to-mass ratio. Because the values of e and Φ of the spacecraft orbits between the two maneuvers have a periodic change, the intersection points of the spacecraft orbits and the Sun-Earth line also have a periodic change. Some spacecraft orbits are shown in Fig 29 and the variation of the distance from the Earth to the intersection points between the two maneuvers is shown in Fig 30.

The bifurcation control completed by changing the area-to-mass ratio cannot change the topology type of the equilibrium point. The controlled spacecraft is stabilized by transferring to the center manifolds of a new stable equilibrium point. This control is achieved by only varying the area-to-mass ratio and the control strategy is very simple. However, this control is instantaneously completed, which requires good respond speed of actuators.

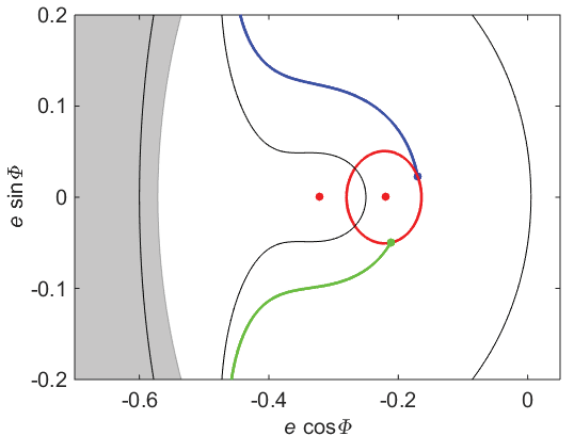

Fig 28. Exploration mission of the magnetic field near the Earth by bifurcation control completed by changing area-to-mass ratio. Spacecraft initial parameters: a=14881 km, e=0.55, Φ=145°, β=10 m^2/kg, α=0°.

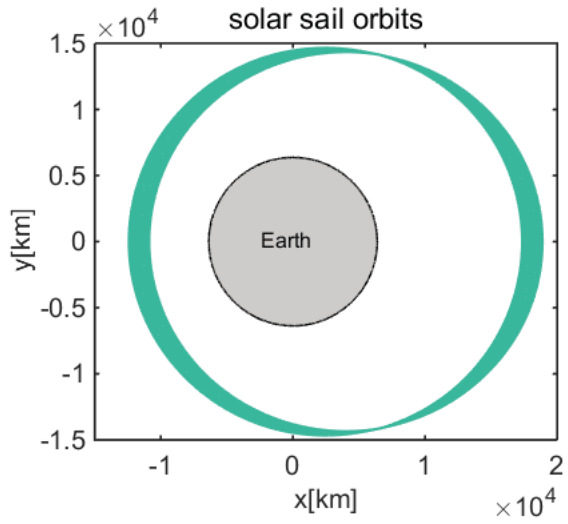

Fig 29. Spacecraft orbits around the Earth between the two maneuvers.

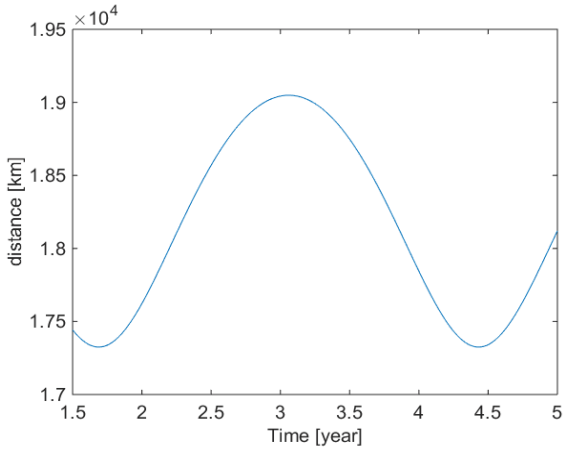

Fig 30. Distance from the Earth to the intersection points between the two maneuvers.

Two HSP controllers are used when the spacecraft is close to a hyperbolic equilibrium point and two bifurcation controllers are used when the spacecraft is close to another stable equilibrium point. Thus, it is impossible to apply the four controllers in the same scenario, i.e., the different equilibrium points that the four controllers work on make their initial parameters different. These application examples demonstrate the feasibility of the controllers in exploring the magnetic field near the Earth. In addition, the qualitative dynamical characteristics of each control can serve as important rules to choose a suitable controller for the given topologic equilibrium points or the usable control variables. From the astrodynamics of viewpoint, the proposed controllers are all feasible. However, as we all know, the selection of controllers is based on not only the astrodynamics, but also other subsystems of the spacecraft, such as TT&C system, thermal control system and power system. This task requires comprehensive analysis from the system engineering viewpoint, thus it should be completed by engineers according to specific mission in the further

research.

5. Conclusion

This paper has studied the orbital dynamics of non-zero attitude angle high area-to-mass ratio spacecraft. This dynamical system allows a maximum of three equilibrium points, one stable at $\Phi=\alpha$, one stable at $\Phi=\alpha+\pi$ and one unstable at $\Phi=\alpha+\pi$. The number of equilibrium points and their eccentricity values depend on semi-major axis a, area-to-mass ratio β, and attitude angle α. The stable equilibrium point at $\Phi=\alpha$ always exists, but the two equilibrium points at $\Phi=\alpha+\pi$ may not exist. For given β and α, the eccentricity values of stable equilibrium point at $\Phi=\alpha$ and unstable equilibrium point at $\Phi=\alpha+\pi$ have a positive relationship with a, while the eccentricity value of stable equilibrium point at $\Phi=\alpha+\pi$ decreases firstly and then increases with the increasing a. For given β and a, the eccentricity values of stable equilibrium point at $\Phi=\alpha$ and unstable equilibrium point at $\Phi=\alpha+\pi$ have a negative relationship with α, while the eccentricity value of the stable equilibrium point at $\Phi=\alpha+\pi$ has a positive relationship with α. For given α and a, the eccentricity values of stable equilibrium point at $\Phi=\alpha$ and unstable equilibrium point at $\Phi=\alpha+\pi$ have a positive relationship with β, while the eccentricity value of the stable equilibrium point at $\Phi=\alpha+\pi$ has a negative relationship with β. In addition, when any two parameters are fixed, five different topologies can successively occur through varying the third parameter. Altogether four different possible behaviors in e_x-e_y phase space are divided by separatrices. The distribution of these behavior areas is corresponding to topologies and vary with the change of β, α and a. Among these five topologies two critical cases where three parameters should meet specific constraint represent the appearance of the bifurcation phenomena.

Three different control methods have been proposed for the stabilization around a hyperbolic equilibrium point. The conventional HSP controller can change the topology type of a hyperbolic equilibrium point from saddle to center. KAM theory guarantees the stability in the sense of Lyapunov. An improved controller was constructed by using further feedback of eccentricity error based on the conventional HSP controller. The topology type of a hyperbolic equilibrium point can be changed from saddle to stable focus, and the system with an improved HSP controller is asymptotically stable. The last way to stabilize the spacecraft near hyperbolic equilibrium point is bifurcation control, which uses topologies and the change of behavior areas. A spacecraft can transfer from behavior III area into behavior IV area by only changing the attitude angle or the area-to-mass ratio.

Non-zero attitude angle high area-to-mass ratio spacecraft has been applied to geomagnetic exploration in this paper. When the area-to-mass ratio and the semi-major axis are set large enough, the natural trajectory around a stable

equilibrium point can be directly used to explore the magnetotail. The spacecraft with a conventional HSP controller can have a bounded trajectory around a hyperbolic equilibrium point. But it is almost impossible to obtain a bounded trajectory which can be completely consistent with the required trajectory. The spacecraft with an improved HSP controller can transfer to the hyperbolic equilibrium point and follow the changing hyperbolic equilibrium points. When the changing trajectory of hyperbolic equilibrium points is designed the same as the required trajectory, the controlled spacecraft will follow the required trajectory. The accelerations required by the conventional HSP controller and the improved HSP controller both should be obtained by orientating the attitude angle and altering the area-to-mass ratio together. Continuously varying the attitude angle and the area-to-mass ratio are necessary to complete these control missions. Because the improved HSP control needs further feedback of eccentricity vector error, in general, lager varying values of the attitude angle and the area-to-mass ratio are needed compared to the conventional HSP control. The spacecraft with bifurcation control can have a bounded trajectory around a new stable equilibrium point. This control is achieved by only varying the attitude angel or the area-to-mass ratio and the control strategy is very simple. However, this control is instantaneously completed, which requires good respond speed of actuators. These qualitative dynamical characteristics of each control can serve as important rules to choose a suitable controller for the given topologic equilibrium points or the usable control variables. However, the task of selecting a controller requires comprehensive analysis from the system engineering viewpoint, thus it should be completed by engineers according to specific mission in the further research.

Acknowledgements

This work was supported by the National Natural Science Foundations of China (11772024 and 11172020); Aerospace Science Foundation by China Aerospace Science and Industry Corporation (170134); Shanghai Space Science and Technology Innovation Foundation (SAST2017-033); the Fundamental Research Funds for the Central Universities (YWF-16-BJ-Y-10); European Research Council (ERC) under the European Union's Horizon 2020 research; and innovation programme (grant agreement No 679086 – COMPASS).

References

[1]. Shapiro, I. I. and Jones, H. M., "Perturbations of the Orbit of the Echo Balloon," *Science*, Vol. 132, No. 3438, 1960, pp. 1484-1486. doi: 10.1126/science.132.3438.1484.

[2]. Musen, P., Bryant, R. and Bailie, A., "Perturbations in Perigee Height of Vanguard I," *Science*, Vol. 131, No. 3404,

1960, pp. 935-936. doi: 10.1126/science.131.3404.935.

[3]. Hamilton, D. P., "Motion of Dust in a Planetary Magnetosphere: Orbit-Averaged Equations for Oblateness, Electromagnetic, and Radiation Forces with Application to Saturn's E Ring," *Icarus*, Vol. 101, No. 2, 1993, pp. 244-264. doi: DOI: 10.1006/icar.1993.1022.

[4]. Krivov, A. V. and Getino, J., "Orbital Evolution of High-Altitude Balloon Satellites," *Astron. Astrophys.*, No. 318, 1997, p. 7.

[5]. Colombo, C., Lücking, C. and McInnes, C. R., "Orbital Dynamics of High Area-to-Mass Ratio Spacecraft with J_2 and Solar Radiation Pressure for Novel Earth Observation and Communication Services," *Acta Astronautica*, Vol. 81, No. 1, 2012, pp. 137-150. doi: 10.1016/j.actaastro.2012.07.009.

[6]. Colombo, C., Xu, M., McInnes, C., "Stabilisation of the hyperbolic equilibrium of high area-to-mass spacecraft," *63rd International Astronautical Congress*, Naples, Italy, IAC-12-C1.1.13 (Oct. 2–6 2012).

[7]. Scheeres, D. J., Hsiao, F.-Y. and Vinh, N. X., "Stabilizing Motion Relative to an Unstable Orbit: Applications to Spacecraft Formation Fight," *Journal of Guidance, Control, and Dynamics*, Vol. 26, No. 1, 2003, pp. 62-73. doi: 10.2514/2.5015.

[8]. Xu, M. and Xu, S., "Structure-Preserving Stabilization for Hamiltonian System and Its Applications in Solar Sail," *Journal of Guidance, Control and Dynamics,* Vol. 32, No. 3, 2009, pp. 997-1004.

[9]. Xu, M., Zhu, J., Tan, T. and Xu, S., "Application of Hamiltonian Structure-Preserving Control to Formation Flying on a -Perturbed Mean Circular Orbit," *Celestial Mechanics and Dynamical Astronomy*, Vol. 113, No. 4, 2012, pp. 403-433.

[10]. Soldini S., Colombo C., Walker. S. J. I., "Solar Radiation Pressure Hamiltonian Feedback Control for Unstable Libration-Point Orbits," *Journal of Guidance, Control, and Dynamics*, Vol. 40, No. 6, 2017, pp. 1374-1389. https://doi.org/10.2514/1.G002090.

[11]. Kokubun, S., Yamamoto, T., Acuña, M. H., Hayashi, K., Shiokawa, K., and Kawano, H., "The GEOTAIL magnetic field experiment," *Journal of geomagnetism and geoelectricity*, Vol 46, No. 1, 1994, pp. 7-22.

[12]. MacDonald, M., and McInnes, C. R., "Geosail: An Enhanced Magnetospheric Mission Using a Small Low Cost Solar Sail," *51st International Astronautical Federation Congress*, IAF Paper 00-W.1.06, Oct. 2000.

[13]. McInnes, C. R., Macdonald, M., Angelopolous, V. and Alexander, D., "Geosail: Exploring the Geomagnetic Tail Using a Small Solar Sail," *Journal of Spacecraft and Rockets*, Vol. 38, No. 4, 2001, pp. 622-629.

[14]. Mengali, G., Quarta, A. A., and Lappas, V. J., "Optimal steering law for the GeoSail mission," *Journal of Guidance Control and Dynamics*, Vol 30, No. 3, 2007, pp. 876-879.

[15]. Lappas, V., Mengali, G., Quarta, A. A., Gil-Fernandez, J., Schmidt, T., and Wie, B., “Practical systems design for an earth-magnetotail-monitoring solar sail mission,” *Journal of Spacecraft and Rockets*, Vol. 46, No. 2, 2009, pp. 381-393.

[16]. Oyama, T., Yamakawa, H. and Omura, Y., “Orbital Dynamics of Solar Sails for Geomagnetic Tail Exploration,” *Journal of Guidance, Control and Dynamics*, Vol. 45, No. 2, 2008, pp. 316-323. doi: 10.2514/1.31274.

[17]. Lücking C., Colombo C., McInnes C. R., "Solar Radiation Pressure-Augmented Deorbiting: Passive End-of-Life Disposal from High-Altitude Orbits", *Journal of Spacecraft and Rockets*, v. 50, n. 6, pp. 1256-1267, Dec. 2013, doi: abs/10.2514/1.A32478, ISSN 0022-4650

[18]. Hamilton, D. P. and Krivov, A. V., “Circumplanetary Dust Dynamics: Effects of Solar Gravity, Radiation Pressure, Planetary Oblateness, and Electromagnetism,” *Icarus*, Vol. 123, No. 2, 1996, pp. 503-523. doi: 10.1006/icar.1996.0175.

[19]. Gómez, G., and Mondelo, J. M., “The dynamics around the collinear equilibrium points of the RTBP,” *Physica D: Nonlinear Phenomena*, Vol. 157, No. 4, 2001, pp. 283-321.

[20]. Gómez, G., Masdemont, J. J., and Mondelo, J. M., “Libration point orbits: a survey from the dynamical point of view,” *Libration Point Orbits and Applications*, 2003, pp. 311-372.

[21]. Hamilton, D. P., and Krivov, A. V., “Dynamics of distant moons of asteroids,” *Icarus*, Vol. 128, No. 1, 1997, pp. 241-249.

[22]. Arnold V. I., Kozlov V. V., and Neishtadt A. I., *Mathematical Aspects of Classical and Celestial Mechanics, 3rd ed*, Springer-Verlag, Berlin, 2006.

[23]. Wiggins S., *Introduction to Applied Nonlinear Dynamical Systems and Chaos, 2nd Ed.*, Springer–Verlag, New York, 2003, Ch. 19.